

# Experimental Investigation of Unsteady Transition Processes on High-Lift T106A Turbine Blades

M. M. Opoka\* and H. P. Hodson†

Whittle Laboratory, Cambridge University, Cambridge, England CB1 0DY, United Kingdom

DOI: 10.2514/1.31947

Periodic wake-boundary layer interactions on the T106A high-lift low-pressure turbine blade cascade at engine-representative flow conditions are described. Through a comparison with previously published moderate Reynolds number/low freestream turbulence data, the influence of elevated freestream turbulence intensity and Reynolds number is assessed and the following conclusions are drawn. At elevated freestream turbulence, the mechanism of turbulence production outside of the boundary layer did not change. Although, an enhanced diffusion of turbulence in the wake was responsible for small decreases in the maximum value of the turbulent kinetic energy in the freestream. For both freestream turbulence cases, the wake from upstream interacted with the inflexional or separated shear layer and forced an inviscid Kelvin–Helmholtz type of breakdown, resulting in the formation of roll-up vortices. At corresponding Reynolds numbers, the turbulence in the wake induced a bypass transition, at a similar streamwise location and phase of the unsteady wake interaction cycle. Furthermore, the higher freestream turbulence delayed the appearance of the inflexional profiles in space, and the transition onset occurred farther upstream. The latter is related with the effect of changes in the Reynolds number. Reduced Reynolds numbers extended the length of the inflexional shear layer, resulting in the formation of a greater number of vortices. Furthermore, the delayed transition allowed these vortices to penetrate farther downstream. Increasing the Reynolds number, at the higher freestream turbulence level, led to the limiting case, where roll-up vortices were not seen to be formed.

## Nomenclature

$C$	=	real blade chord
$C_p$	=	pressure coefficient
$F_{red}$	=	reduced frequency
$f$	=	frequency
$H$	=	shape factor
$h$	=	blade span
$P$	=	pressure
$Re$	=	Reynolds number
$s$	=	blade pitch
$\overline{U}$	=	speed
$\overline{u'^2}, \overline{v'^2}$	=	Reynolds normal stresses
$\alpha$	=	flow angle
$\delta^*$	=	displacement thickness
$\eta$	=	weighting factor
$\theta$	=	momentum thickness
$\tau$	=	time or shear stress
$\phi$	=	flow coefficient

## Subscripts

bar	=	referred to bar speed
is	=	isentropic
max	=	maximum
min	=	minimum
$s$	=	static
$w$	=	wall
0	=	total
1, 2	=	inlet and outlet

Presented as Paper 1227 at the XVII International Symposium on Air Breathing Engines, Munich, Germany, 4–9 September 2005; received 4 May 2007; revision received 13 September 2007; accepted for publication 4 October 2007. Copyright © 2007 by the American Institute of Aeronautics and Astronautics, Inc. All rights reserved. Copies of this paper may be made for personal or internal use, on condition that the copier pay the \$10.00 per-copy fee to the Copyright Clearance Center, Inc., 222 Rosewood Drive, Danvers, MA 01923; include the code 0748-4658/08 \$10.00 in correspondence with the CCC.

\*Ph.D. Student; currently at Rolls-Royce Deutschland; maciej.opoka@rolls-royce.com.

†Professor of Aerodynamics, Engineering Department; hph1000@cam.ac.uk.

## I. Introduction

THE relative motion of the adjacent blade rows in turbomachines gives rise to a variety of unsteady interactions. The potential influence of a blade extends both upstream and downstream. It decays exponentially with a length scale of the order of the blade pitch. Wakes appear as the boundary layers from upstream blades are convected downstream. Their rate of decay is much lower than that of the potential influence. As a result, the interaction of wakes with downstream blade rows has received far more attention in the literature. Much of this work has been concerned with the effect of the velocity and turbulent fluctuations on the laminar-turbulent transition processes within the suction side boundary layer. This is important because the suction side boundary layers are responsible for most of the loss of efficiency (Curtis et al. [1]).

It is believed that wake-induced transition in low-pressure (LP) turbines may occur in one of three ways (Halstead et al. [2]) by one of three mechanisms. If the Reynolds number is high enough such that transition is completed before laminar separation can occur, or if the boundary layer does not separate because the levels of suction-surface deceleration are slight, then attached flow transition is induced by the high turbulence in the wakes. This is bypass transition. It begins with the formation of turbulent spots in the otherwise laminar boundary layer. Between the wakes, the flow also remains attached. Farther downstream, the background disturbances may also promote transition between the wake-induced events as these propagate downstream. This is sometimes referred to as a natural mode of transition.

If the suction-surface deceleration is more severe and/or the Reynolds number is low, then the laminar boundary layer tends to separate and wake-induced transition occurs in the free shear layer of a separation bubble. Such a process was observed by Stieger and Hodson [3] who, using a low-speed facility, observed an additional aspect to the transition mechanism on the high-lift T106 LP turbine blade. The inviscid Kelvin–Helmholtz interaction occurred due to the wake velocity fluctuations acting on the separated inflexional boundary layer velocity profile. This led to the shear layer rolling up into a row of coherent structures. A similar behavior was later observed in high-speed turbine cascade tests conducted by Vera et al. [4] and in compressor tests by Hilgenfeld and Pfitzner [5]. In the case of Stieger and Hodson [3], this mechanism preceded the transition induced by the turbulence in the wake.

At intermediate Reynolds numbers, the wakes induce transition in the attached flow ahead of where the laminar boundary layer would separate in steady flow. If the frequency of the incoming wakes is not too high, the boundary layer can separate and undergo transition in the separated shear layer between the wake-affected events. This is more likely to occur in high-lift designs.

One more aspect of wake-boundary layer interaction should be mentioned in the context of profile loss. The so-called calmed region, which trails the turbulent spots, was identified first by Schubauer and Klebanoff [6]. This region is characterized by full velocity profiles and therefore has an elevated wall shear stress. These characteristics mean that the calmed flow can withstand more diffusion on the blade suction surface than a normal laminar boundary layer (Schulte and Hodson [7]). This has led to the design of blades of higher lift without the development of a significant suction-side separation bubble.

Most of the published research into wake-boundary layer interactions has been carried out at levels of freestream turbulence intensity below 2%. This has been successful because the wakes contain relatively high levels of turbulence, which dominate the transition process. However, this is not fully representative of real engine conditions. The turbulence intensity in a multistage low-pressure turbine has been measured by Halstead [8]. He reported that the midspan turbulence intensity levels varied between 2 and 5% in the “freestream.” Binder et al. [9] who performed tests at relatively low Reynolds numbers, where the blade surface flow was separated at the trailing edges, reported that the maximum turbulence intensity within the wake of the nearest upstream blade row did not exceed 10%.

The work presented in this paper describes the experimental investigations of the effects of inlet freestream turbulence and flow Reynolds number on the transition process on a high-lift LP turbine cascade.

## II. Experimental Setup

The general arrangement of the test facility is shown in Fig. 1. The basic rig characteristics are summarized in Table 1. The cascade (1) consists of six T106 profiles, assembled with a pitch-chord ratio to give the configuration known as “T106A.” The upstream moving bar system (2) is used to generate the wakes. The downstream system (3) was not used in the current work. The upstream bar system was driven by a 2.3 hp ac motor (4) with feedback control. The test facility was attached to the outlet of the open cycle low-speed wind tunnel. A centrifugal fan supplied the airflow to the wind tunnel. The set of gauzes and honeycomb inserts in the tunnel made the flow uniform before delivering it into the cascade test section through the inlet duct (7). The airflow from the wind tunnel is characterized by low turbulence levels of the order of 0.5%. To reach levels of inlet freestream turbulence intensity that are more representative of the multistage environment a turbulence grid was used. The design of the turbulence grid (8) was based on the work of Roach [10]. The grid was located at a distance of three axial chords upstream of the test blade (9) and provided an inlet turbulence intensity of 4.0% at the location corresponding to the leading edge of the test blade. The associated turbulence (integral) macrolength scale, representative of the largest eddies in the turbulent flow was equal to  $0.076C_{ax}$ , while the microlength scale responsible for dissipation was  $0.018C_{ax}$ .

Total and static pressure probes at the inlet to and wall tapings at the outlet from the cascade were used to monitor the flow conditions and to check the level of inlet uniformity and outlet periodicity. Adjustable tailboards (10), shown in Fig. 1, extending from the trailing edge of the top and bottom blades were used to ensure that the outlet flow was periodic.

### A. Measurements and Flow Conditions

The cascade flow conditions were monitored with a 16-channel Scanivalve DSA 3107. The T106 test blade (9) shown in Fig. 1 was equipped with surface pressure tappings. The tappings had a diameter of 0.3 mm and were located at 45% of the blade span. Time mean levels of surface static pressure were measured using a Scanivalve system. Surface flush-mounted, fast response Kulite

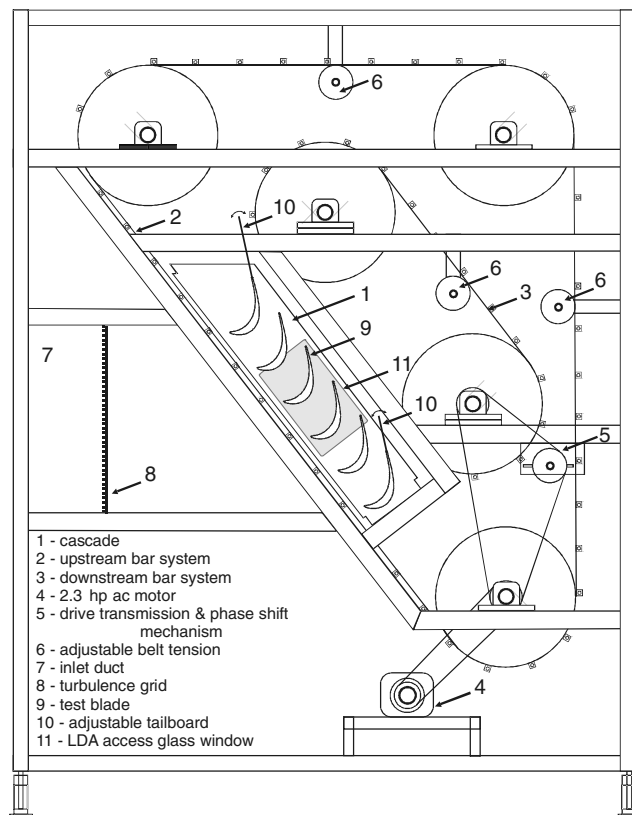


Fig. 1 Schematic of T106A test facility.

pressure transducers (model XCS-062) were used to acquire unsteady suction-surface pressures at blade midspan. A detailed description of the Kulite signal acquisition procedure may be found in Stieger et al. [11]. A sheet of 50 hot film sensors spaced at intervals of 2.54 mm in the streamwise direction was fitted on the blade suction surface at midspan. The array was manufactured by Senflex. The sensors were used to measure the quasi-wall shear stress distribution using the procedure described in Hodson et al. [12]. Each sensor was connected to a Dantec C-series anemometer. The signal outputs from each anemometer were first acquired with filter settings that provided only the mean component. Then, a bandpass filter was used to acquire the fluctuating component.

During the acquisition of the hot film and pressure transducer data, the logging frequency was 10 kHz and 128 ensembles of 4096 samples were acquired. The data in this paper are presented as a pressure coefficient or as a normalized quasi-wall shear stress. These are defined by Eqs. (1) and (2), respectively,

$$C_{p2is} = \frac{P_{01} - P_{S(s)}}{P_{01} - P_{S2}} \quad (1)$$

Table 1 Characteristic of T106A test facility

Cascade properties	
Profile	T106
No. of blades in the cascade	6
Real chord $C$ , mm	198
Axial chord $C_{ax}$ , mm	170
Cascade pitch $s$ , mm	158.2
Pitch-to-chord ratio $s/C = \tau$	0.799
Blade aspect ratio $h/C$	1.884
Design inlet flow angle $\alpha_1$ , deg	-37.7
Design exit flow angle $\alpha_2$ , deg	63.2
Upstream bar diameter $d$ , mm	2.05
Upstream bar to leading edge, mm	70
Upstream bar pitch, mm	158.2

$$\langle \tau_w \rangle_{ND} = \frac{\langle \tau_w(s) \rangle - \langle \tau_w(s) \rangle_{\min}}{\langle \tau_w(s) \rangle_{\max} - \langle \tau_w(s) \rangle_{\min}} \quad (2)$$

$$\eta_i = \frac{t_{ri}}{\sum_{j=1}^N t_{rj}} \quad (3)$$

$$\bar{u} = \sum_{i=1}^N \eta_i u_i \quad (4)$$

$$\overline{u^2} = \sum_{i=1}^N \eta_i (u_i - \bar{u})^2 \quad (5)$$

$$\overline{u'v'} = \sum_{i=1}^N \eta_i (u_i - \bar{u})(v_i - \bar{v}) \quad (6)$$

$$Re_{2, \text{is}} = \frac{\rho V_{2, \text{is}} \cdot C}{\mu} \quad (7)$$

$$\phi = \frac{V_{x1}}{U_{\text{bar}}} \quad (8)$$

$$F_{\text{red}} = \frac{f \cdot C}{V_{2, \text{is}}} \quad (9)$$

One of the cascade sidewalls was equipped with a glass window (11) to allow laser beam access (see Fig. 1). Two-dimensional laser Doppler anemometry (LDA) blade passage and suction-surface boundary layer surveys were performed using a 5-W argon ion laser (Coherent Innova 70) and Dantec FiberFlow System with a beam expander. The size of the measuring volume was equal to approximately  $0.08 \times 0.08 \times 1.00$  mm. The laser signal acquisition system was operated in backscatter mode. The Dantec Burst Spectrum Analyzers (BSA) and photomultiplier tubes were controlled with LabVIEW software. The acquisition was triggered with each bar passing event. Data were collected in the dead time mode with a dead time interval that ensured the statistical independence of the acquired data.

The seeding for the LDA was generated using a TSI Six Jet Atomizer with Shell Odina Oil. The particle size was approximately  $1.5 \mu\text{m}$ . The data rate during the acquisition varied between 1.5 and 5 kHz. During the postprocessing of laser signals a coincidence filter was used. The coincidence window was set to 0.005 ms. The velocity bias resulting from periods of higher or lower velocity was removed using a residence time weighting factor as defined in Eq. (3) (see George [13]).

The LDA data were ensemble averaged by first dividing the wake passing period into 128 time bins. Each time bin was evaluated based on a nominal average of 500 samples. The weighting factor, mean, variance, and cross moments were then calculated for each time bin according to Eqs. (3–6).

Tests were performed at three Reynolds numbers ( $0.9$ ,  $1.6$ , and  $2.6 \times 10^5$ ) based on the exit isentropic velocity and the real chord as given by Eq. (7). The flow coefficient, defined by Eq. (8), was equal to  $0.83$ . The reduced frequency of the passing wakes, defined by Eq. (9), was set to  $0.68$ . The background flow was characterized by two levels of inlet freestream turbulence intensity ( $Tu_1 = 0.5\%$  and  $4.0\%$ ).

### B. Uncertainty Analysis

At the exit from the cascade, the exit dynamic pressure varied by less than  $2.5\%$  over the five passages. Over the central passages, the variation was less than  $1\%$ .

The inclination of the laser probe with respect to the suction surface of the blade was of the order of  $5$  deg. This was to avoid any obstruction of the laser beams by the blade wall. The velocity measured with the inclined LDA probe is insignificantly different from that measured with a noninclined probe (less than  $0.5\%$ ) and for this reason it was considered unnecessary to apply a correction to the measurements. The step resolution of the traversing system was  $0.025$  mm.

The mean pressure levels were measured using a Scanivalve DSA 3107 array with a  $\pm 2500$  Pa range. The discretization error on this measurement is  $0.17$  Pa, which corresponds to  $0.2\%$  of the exit dynamic pressure at  $Re_{2, \text{is}} = 1.6 \times 10^5$ . The sensitivity of the Kulite transducer system was approximately equal to  $500$  Pa/V with a discretization error of  $0.05$  Pa.

## III. Steady Flow Results

### A. Surface Pressure Coefficient

The measured steady-state distributions of the surface pressure coefficient at datum Reynolds number ( $Re_{2, \text{is}} = 1.6 \times 10^5$ ) are presented for both cases of inlet turbulence intensities ( $Tu_1 = 0.5\%$  and  $4.0\%$ ) in Fig. 2. The peak suction position occurred for both cases at a surface position of  $s/S_0 = 0.44$ . From this point, the boundary layer flow decelerates under the influence of an adverse pressure gradient.

In the case of the lower freestream turbulence, the suction-surface boundary layer was observed to separate at a surface distance of  $s/S_0 = 0.63$ . From this point, the pressure “plateau” extended up to a distance of  $s/S_0 = 0.83$ . The end of the pressure plateau indicates the onset of the transition process, allowing the surface pressure to recover. At a surface distance of  $s/S_0 = 0.9$ , the boundary layer was attached.

In the case of the higher freestream turbulence, the distribution of the surface pressure coefficient at surface distances between  $s/S_0 = 0.6$  and  $s/S_0 = 0.8$  lacks the pressure plateau. This suggests the absence of the separation bubble due to attached flow transition.

The lines imposed above the previously described complete pressure distributions in Fig. 2 illustrate the effect of varying the Reynolds number at the lower level of inlet freestream turbulence intensity. Only the rear portion of the suction-surface distribution ( $s/S_0 = 0.49$ – $1.0$ ) is represented, as the main differences appear in this region. As the Reynolds number decreases, the extent of the separation bubble grows. This is because the onset of transition in the separated shear layer occurs farther downstream.

### B. Boundary Layer Integral Parameters

The boundary layer integral parameters calculated from the LDA data measured with a freestream turbulence intensity of  $0.5\%$

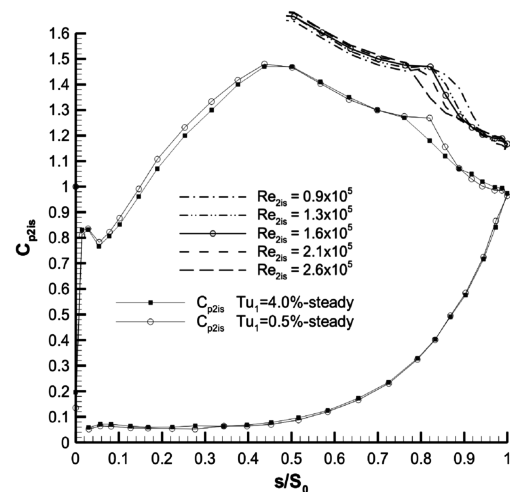


Fig. 2 Steady-state surface pressure coefficient for  $Tu_1 = 0.5\%$  at  $Re_{2, \text{is}} = 0.9 \times 10^5$ ,  $1.3 \times 10^5$ ,  $1.6 \times 10^5$  (complete), and  $2.1 \times 10^5$ ,  $2.6 \times 10^5$ , for  $Tu_1 = 4.0\%$  at  $Re_{2, \text{is}} = 1.6 \times 10^5$  (complete).

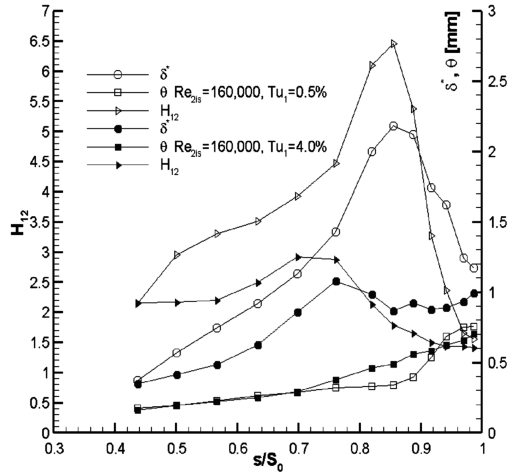


Fig. 3 Steady-state suction-surface boundary layer integral parameters for  $Tu_1 = 0.5\%$  and  $Tu_1 = 4.0\%$  at  $Re_{2is} = 1.6 \times 10^5$ .

(hollow symbols) and 4.0% (filled symbols) are shown in Fig. 3. For the lower turbulence intensity case, at a surface distance of  $s/S_0 = 0.63$ , the laminar boundary layer separates with a shape factor ( $H_{12}$ ) of 3.5. Downstream of this separation point, the displacement thickness continues to rise, until a surface distance of  $s/S_0 = 0.85$ . The momentum thickness ( $\theta$ ) increases slowly in this region, which corresponds with the pressure plateau in Fig. 2. At a surface distance of  $s/S_0 = 0.83$ , the pressure plateau terminates and the surface pressure begins to recover. This is followed by the rapid increase of momentum thickness which ends at the surface position

of  $s/S_0 = 0.94$ . This indicates the end of the transition process. The boundary layer leaving the blade trailing edge is attached and fully turbulent ( $H_{12} < 1.6$ ).

For the case of the higher freestream turbulence intensity, the transition process differs. The higher levels of freestream disturbance enhance the exchange of energy between the freestream and the boundary layer region. The boundary layer flow, after passing the point of the peak suction, is therefore characterized by a lower displacement thickness ( $\delta^*$ ) even though it experiences a similar adverse pressure gradient. On the other hand, the momentum thickness shows no sensitivity to freestream turbulence over the distance  $s/S_0 = 0.44-0.70$ . At a surface distance of  $s/S_0 = 0.70$  the curve of the momentum thickness representing the higher turbulence intensity case departs from the curve of the lower freestream turbulence. This rise of momentum thickness indicates that the transition process has begun. Therefore, it seems that the suction-surface boundary layer at the higher turbulence intensity level, although inflexional, will not undergo separation, as was observed in the lower freestream turbulence case. In fact, the boundary layer shape factor does not exceed a value of 3.0.

#### IV. Unsteady Flow Results

##### A. Measurements of Wake Convection in the Blade Passage

Stieger and Hodson [14] previously performed a 2-D LDA survey in the T106A blade passage at  $Re_{2is} = 1.6 \times 10^5$  with the lower freestream turbulence intensity ( $Tu_1 = 0.5\%$ ). Figure 4 shows their contours of ensemble-averaged nondimensional turbulent kinetic energy (TKE) at six equally spaced instants during the one wake passing period. The turbulent kinetic energy was calculated from the measured velocity variance components normalized by  $V_{2is}^2$  according to Eq. (10):

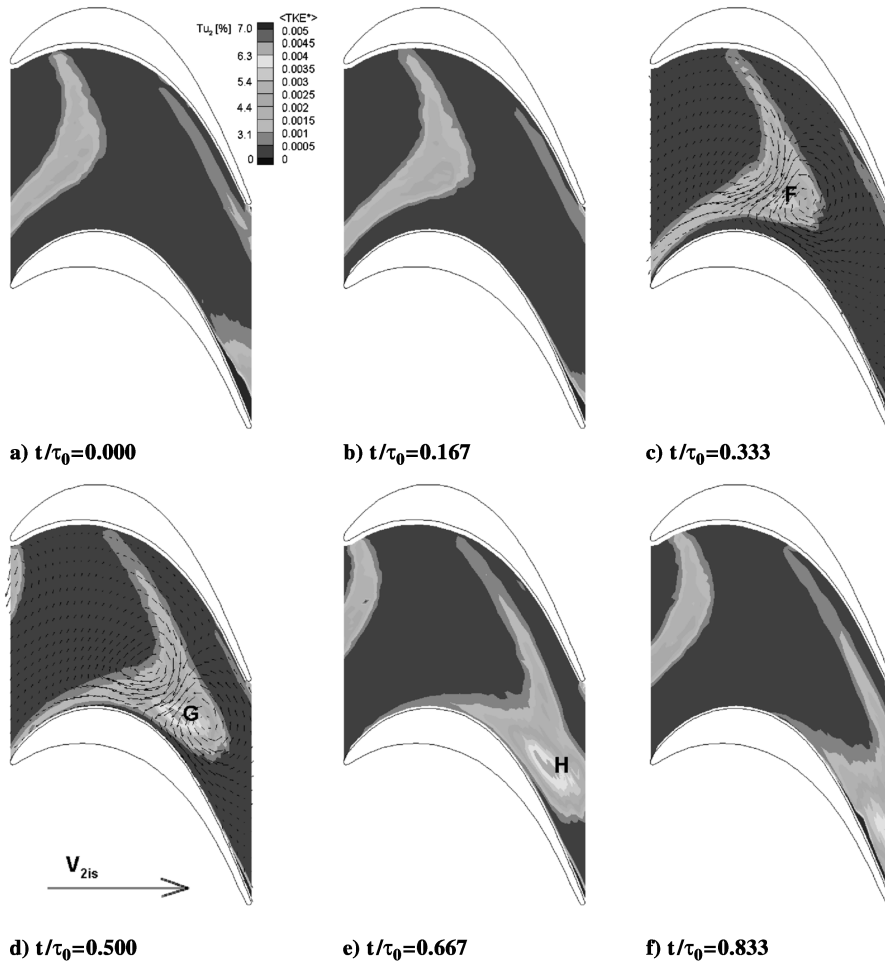


Fig. 4 Measured TKE and velocity perturbation vectors in a T106A blade passage at  $Re_{2is} = 1.6 \times 10^5$  and  $Tu_1 = 0.5\%$  (Stieger and Hodson [14]).

$$\langle \text{TKE}^* \rangle = \frac{1}{2}(\overline{u^2} + \overline{v^2}) \quad (10)$$

For two time instants, the velocity perturbation vectors have been imposed on the contour field to illustrate the negative jet effect of the wake. The kinematic convection of the wake is apparent, with the wake clearly distinguished from the background flow by high levels of TKE.

Along the pressure side of the channel, the TKE of the wake fluid is observed to drop as it convects through the blade passage. A combination of elongation of the wake centerline and, to a lower extent, the convective transport away from the pressure surface (due to the negative jet) is responsible for this reduction in TKE. Similarly, stretching causes the TKE to reduce over the forward part of the suction surface (see Figs. 4c and 4d). The highest levels of TKE outside of the boundary layer occur in Figs. 4d and 4e. These high regions of TKE, labeled G and H, occur where the wake fluid accumulates near the suction surface. The perturbation velocity vectors superimposed in Fig. 4d indicate that the peak TKE occurs slightly below the centers of the counter rotating flow. These high levels of TKE originate from the enhanced production of TKE, which occurs when the turbulence extracts the work from the mean flow in regions having high turbulent stresses and high spatial velocity gradients. The turbulent stresses are confined to the wake fluid and so the production occurs when the wake enters the region of high spatial velocity gradients.

The turbulence intensity levels that correspond to particular TKE values are given in the figure legend. Again, these are normalized by the exit velocity and not the local velocity. In the freestream, the wake entering the blade passage is characterized with turbulence intensity of the order of 4.5%. The maximum turbulence intensity observed in the core of spots labeled G and H was equal to 6.5%. However, the part of the wake in direct contact with the region of

suction surface where the separation was observed is characterized by turbulence intensity of the order of 3 to 4%.

As highlighted in the Introduction, in real multistage LP turbines, the reported levels of measured freestream turbulence intensity range between 2 and 5%. In Fig. 5, the results of the current 2-D LDA survey in the T106A blade passage at  $Re_{2is} = 1.6 \times 10^5$  with the higher freestream turbulence intensity ( $Tu_1 = 4.0\%$ ) are presented. There is an obvious increase in the background level of turbulent kinetic energy. The data were again normalized with the exit velocity. One may observe that the background level of turbulence in the blade passage is equal approximately to  $Tu_2 = 2.6\%$ , which is equivalent to  $Tu_1 = 4.0\%$ . The wake structure at particular instants during the wake period does not significantly differ from that observed at the lower turbulence level. As previously observed, points G and H in the freestream are characterized by the highest levels of TKE. These regions appear at the same time instants  $t/\tau_0 = 0.500$  and  $t/\tau_0 = 0.667$  as in Figs. 4d and 4e. The maximum levels are comparable; a small decrease of TKE in the center of regions labeled G and H occurs due to the higher background turbulence, which is responsible for a higher degree of turbulent diffusion in the wake core. Therefore, the turbulent stresses in the wake are spread over a larger area before it enters the region of high spatial velocity gradients. The levels of the turbulence intensity in the wake above the rear part of the suction surface (i.e., where transition occurs) are of the order of 4 to 5%.

## B. LDA Survey of Suction-Surface Boundary Layer

The effect of freestream turbulence on the wake-boundary layer interaction was investigated using the LDA technique. Figures 6 and 7 illustrate the unsteady distribution of the boundary layer shape factor along the rear part of the blade suction surface in the form of

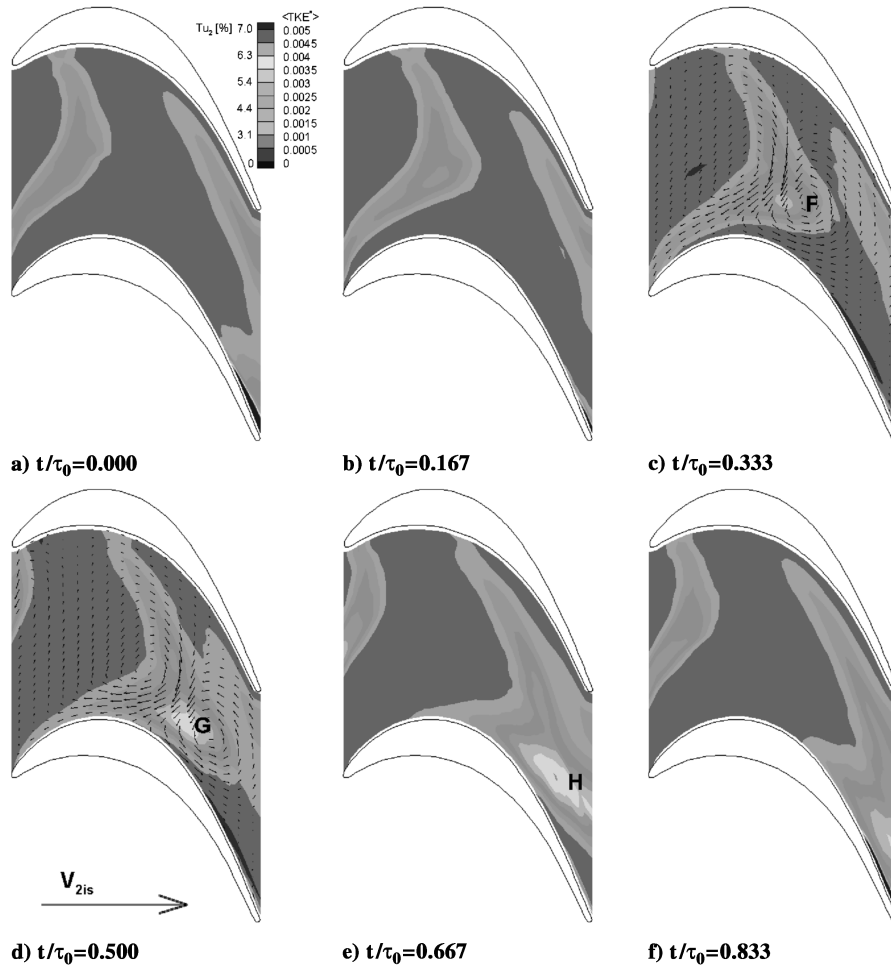
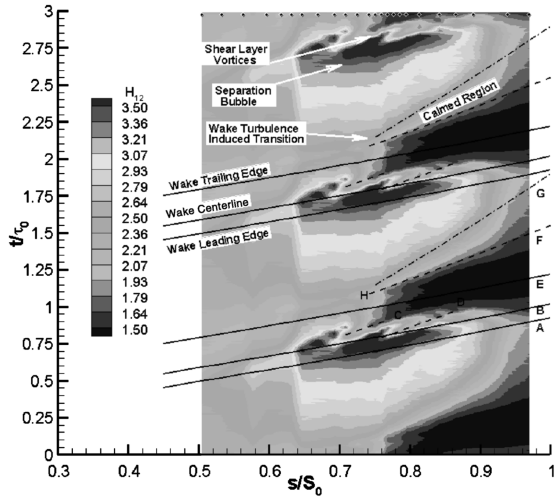
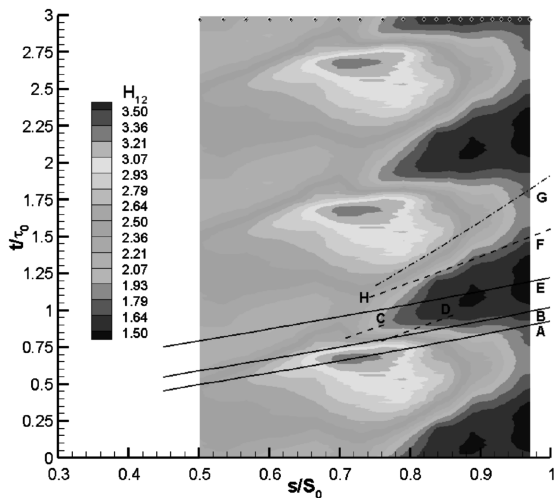


Fig. 5 Measured TKE and velocity perturbation vectors in a T106A blade passage at  $Re_{2is} = 1.6 \times 10^5$  and  $Tu_1 = 4.0\%$ .



**Fig. 6** Distance-time plot of the suction-surface ensemble-averaged boundary layer shape factor ( $H_{12}$ ) measured at  $Re_{2is} = 1.6 \times 10^5$ ,  $Tu_1 = 0.5\%$ , and  $F_{red} = 0.68$  by Stieger and Hodson [3].



**Fig. 7** Distance-time plot of the suction-surface ensemble-averaged boundary layer shape factor ( $H_{12}$ ) measured at  $Re_{2is} = 1.6 \times 10^5$ ,  $Tu_1 = 4.0\%$ , and  $F_{red} = 0.68$ .

space time (ST) diagrams. Dots, shown at the top of the contour field, indicate the traverse position. Solid lines (A, B, and E) superimposed on the contour field represent the location of the leading edge, center, and trailing edge of the wake. The trajectory of these lines was calculated from the measured steady-state surface pressure coefficient data and corresponds to the freestream velocity. The wake leading edge line (A) represents the path along which the periodic velocity perturbation reaches its maximum positive value. The wake trailing edge line (E) represents the path along which periodic velocity perturbation reached its maximum negative value. The centerline of the wake (B) is identified with the occurrence of a perturbation from the mean of zero velocity between the minimum and maximum values associated with lines A and E.

The data presented in Fig. 6 were acquired by Stieger and Hodson [3]. In Fig. 6, the wake passing over the suction surface was found to periodically suppress the separation bubble. The regions of separation are indicated by the islands of high values of the shape factor ( $H_{12} > 3.2$ ). Furthermore, the behavior of the wake negative jet was reported to have forced the inflexional and separated shear layer to roll up into a row of spanwise vortices. Once formed, these vortices were found to travel downstream at half of the freestream velocity.

In Fig. 6, between lines B and E, the downstream traveling roll-up vortices cause the variation of the shape factor seen between lines C

and D. Beneath the roll-up vortices low values of the shape factor indicate the turbulent character of the boundary layer. These regions of low shape factor join with the turbulent wedge formed between lines E and F representing the region of wake-induced bypass transition. This bypass transition was induced by the wake turbulence. This bypass transition was induced by the wake turbulence induced transition is followed by the calmed flow inside the wedge formed between lines F and G. In this region, the shape factor progressively recovers from turbulent to laminarlike values. The decay of the calmed region is followed by the reestablishment of the separation bubble and high values of the shape factor.

In Fig. 7, the effect of the increased level of inlet freestream turbulence intensity on the distribution of the boundary layer shape factor is illustrated. Steady-state observations showed that the higher turbulence levels in the freestream prevented the shape factor from exceeding a value of 3. Therefore, the laminar separation was not present.

In the case of the unsteady flow, the boundary layer shape factor has similar maximum values of about 3.2. In fact, these occur only in a narrow region at a surface distance between  $s/S_0 = 0.70$  and  $s/S_0 = 0.76$ , beneath line A. This region is believed to result from the effect of the negative jet along line A. Although the velocity profiles are inflexional, neither reverse flow, nor evidence of shear layer roll-up vortices was observed in the region between lines B and E in Fig. 7.

The remaining effects associated with the wake appeared at similar streamwise locations as observed in Fig. 7. The turbulence in the wake induced bypass transition at point H. This is because distributions of the Reynolds number based on the momentum thickness behind line E at both cases of inlet turbulence intensity are similar. Furthermore, as observed previously in Fig. 6, the wedge of the wake-induced transition (between lines E and F) merged with the turbulent flow formed between lines B and E. The calmed region between lines F and G in Fig. 7 shows similar levels of the shape factor as in the case of the lower freestream turbulence.

### C. Unsteady Suction-Surface Pressure Coefficient

In Fig. 8, the unsteady distribution of the suction-surface pressure coefficient [see Eq. (1)] at the lower level of turbulence intensity is presented in the form of an ST diagram. These data were measured by Stieger et al. [11], with fast response pressure transducers. (Figures 8–11 are drawn with the data grid skewed so that the abscissa is parallel to a line drawn at half of the mean velocity. This reduces the aliasing in the contour algorithm that results from the temporal resolution being much finer than the spatial resolution.) The presence of the shear layer vortices is indicated by rapid changes of pressure coefficient at surface positions between  $s/S_0 = 0.6$  and  $s/S_0 = 0.9$ . The downstream traveling vortices are responsible for phase-averaged surface pressure oscillations of the order of 30% of the exit dynamic pressure peak to peak.

In Fig. 9, the unsteady distribution of the suction-surface pressure coefficient at the elevated level of inlet freestream turbulence ( $Tu_1 = 4.0\%$ ) is presented. Data were only acquired downstream of a surface distance of  $s/S_0 = 0.567$ . This is because, until this location, the unsteady pressure data are essentially the same for both levels of the inlet freestream turbulence intensity. In the case of the higher freestream turbulence, the maximum values of the phase-averaged surface pressure oscillations were of the order of just 10% of the exit dynamic pressure peak to peak. A similar order of magnitude of peak-to-peak values was reported by Stieger et al. [11] in the case of a tripped boundary layer. In that case, roll-up vortices were not formed and the transition proceeded in the attached flow. In Fig. 9 however, a short event is observed between lines B and E, at a surface distance between  $s/S_0 = 0.64$  and  $s/S_0 = 0.72$ , which has a similar nature to that of the shear layer roll-ups described in the case of Fig. 8. Although this observation does not explain the mechanism of transition between lines B and E, it suggests that in the shear layer a roll-up vortex might be forming.

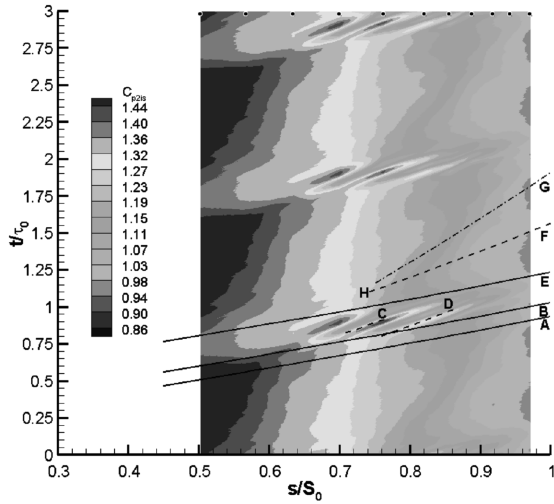


**Fig. 8** Distance-time plot of the suction-surface pressure coefficient ( $C_{p2is}$ ) measured at  $Re_{2is} = 1.6 \times 10^5$ ,  $Tu_1 = 0.5\%$ , and  $F_{red} = 0.68$  by Stieger and Hodson [14].

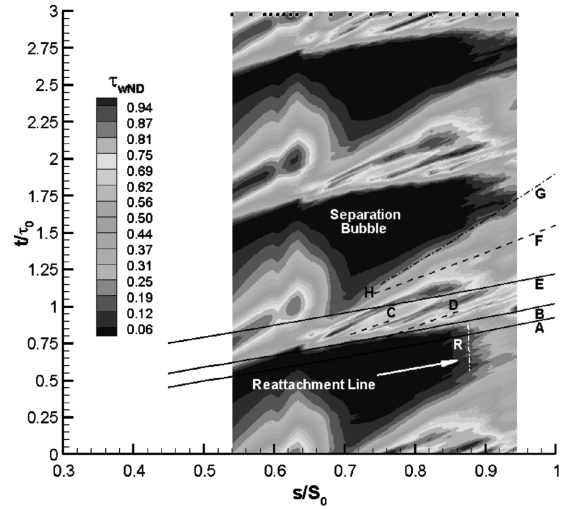


**Fig. 10** Distance-time plot of the suction-surface ensemble-averaged normalized quasi-wall shear stress ( $\tau_{wND}$ ) measured at  $Re_{2is} = 1.6 \times 10^5$ ,  $Tu_1 = 0.5\%$ , and  $F_{red} = 0.68$ .

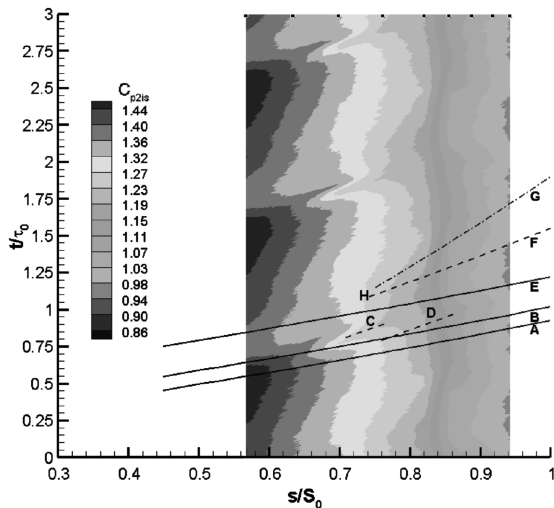


**Fig. 9** Distance-time plot of the suction-surface pressure coefficient ( $C_{p2is}$ ) measured at  $Re_{2is} = 1.6 \times 10^5$ ,  $Tu_1 = 4.0\%$ , and  $F_{red} = 0.68$ .

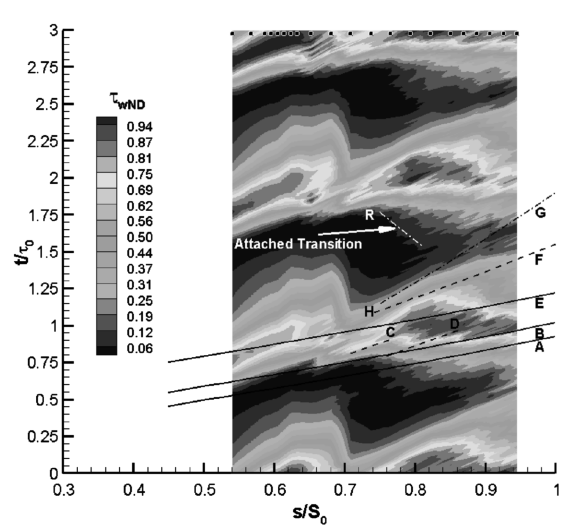


**Fig. 11** Distance-time plot of the suction-surface ensemble-averaged normalized quasi-wall shear stress ( $\tau_{wND}$ ) measured at  $Re_{2is} = 1.6 \times 10^5$ ,  $Tu_1 = 4.0\%$ , and  $F_{red} = 0.68$ .

#### D. Unsteady Suction-Surface Quasi-Wall Shear Stress

To gain further insight into the time history of the near wall flow along the rear part of the suction surface, an array of hot film shear stress sensors was fitted on the blade surface. The normalized ensemble-averaged quasi-wall shear stress [see Eq. (2)] is presented in Figs. 10 and 11. The normalization of hot film signals is performed for each sensor independently. The resulting values vary from 0 to 1. This form of presentation emphasizes the periodic fluctuations at the expense of providing data on the changes in the mean level. Figure 10 corresponds to the results presented in Figs. 6 and 8 ( $Tu_1 = 0.5\%$ ). Data shown in Fig. 11 were measured at the higher level of the inlet freestream turbulence ( $Tu_1 = 4.0\%$ ), and correspond with Figs. 7 and 9.

At the lower inlet freestream turbulence intensity (Fig. 10), the unsteady boundary layer was laminar up to a surface distance of  $s/S_0 = 0.63$ , which is the location of the steady-state onset of separation (see Fig. 2). In Fig. 10, downstream of this location at point H, the turbulence in the wakes was found to periodically induce laminar-turbulent transition. This creates the region bounded by lines E and F. The region of wake-induced transition is followed by a calmed region between lines F and G. The calmed region has an elevated wall shear stress, which reduces in value from that of a turbulent to the level of a laminar separated flow as time progresses, as described by Schulte and Hodson [7]. In the path between the wakes, the boundary layer was separated. This is indicated by the

very low values of the normalized quasi-wall shear stress. The increased levels of the shear stress along line R indicate the position of the reattachment of this part of the flow.

The roll-up vortices described in the previous section can also be identified in Fig. 10 by the patterns of low and high shear stress starting from  $s/S_0 = 0.65$ , between lines B and E. The dashed lines C and D are reproduced from Fig. 6. These indicate the paths along which the vortices were moving. Above line E, which indicates the leading edge of wake-induced transition, vortices cannot be identified. This may be because turbulent flow inside the wedge that is formed between lines E and F overtakes and corrupts the slowly moving vortices or because the vortices themselves break down into turbulence. This corresponds to the merging of the low shape factor regions due to wake-induced transition and due to shear layer vortices that can be seen in Fig. 6.

Figure 11 presents an ST diagram of the normalized ensemble-averaged quasi-wall shear stress at the inlet freestream turbulence intensity of 4.0%. At this flow condition, the onset of the transition in the region between the wakes occurs farther upstream. Line R, following the earlier appearance of the region of higher shear stress has moved upstream. In addition, line R is also inclined. This is believed to result from the effect of the calmed region delaying the transition onset between the wake events.

In Fig. 11, between lines B and E at surface distances between  $s/S_0 = 0.7$  and  $0.8$ , a pattern of a high and a low wall shear stress appears along line C. Though less distinct, this resembles the pattern in Fig. 10 associated with the passage of the shear layer roll-up vortices. In Fig. 11, the pattern appears only for a short time.

Stieger and Hodson [14] highlighted the fact that the frequency of the detected roll-up vortices is near to the frequency of the most amplified instability waves given by Eq. (11):

$$f = \frac{3.2U_\infty^2 \text{Re}_{\delta^*}^{-3/2}}{2\pi\nu} \quad (11)$$

which was published by Walker [15]. The frequency calculated from the above equation for the steady-state boundary layer at the surface position  $s/S_0 = 0.63$  is equal to approximately 330 Hz for the lower freestream turbulence intensity case. The wake enters the blade passage at the frequency of 42 Hz. The extent of the wake's negative jet on the suction surface (time between lines A and E) constitutes 30% of the wake period. Therefore, between two and three cycles of fluctuations at the frequency of the most amplified instability waves may occur under the passing wake. At these moderate Reynolds numbers, when analyzing particular ensembles of the raw pressure or hot film signals, it was observed that the number of generated vortices varied from 1 to 3 at the lower turbulence intensity case, whereas for the case of the higher freestream turbulence only an occasional singular vortex was seen.

The shear layer vortices were not observed at the higher freestream turbulence in the LDA data in Fig. 7. This is believed to be due to an unfortunate streamwise distribution of traverse positions. However, a small perturbation in wall normal velocity component, characteristic of a roll-up vortex, was observed inside the boundary layer at a surface distance of  $s/S_0 = 0.73$ , along path C. The formation of a possible roll-up vortex was indicated in the unsteady pressure data of Fig. 9. In Fig. 11, a strip of higher wall shear stress moves along the trajectory line C. This trajectory corresponds to half of the freestream velocity and the typical speed for shear layer vortices. This might serve as further evidence for the presence of a roll-up vortex. Furthermore, the observed amplitude of the pressure oscillation suggests that the size of this shear layer vortex is reduced.

### E. Unsteady Suction-Surface Pressure Signals

Up to this point, only the effect of inlet freestream turbulence has been discussed. Here, this effect will be compared to the effect of changing the Reynolds number.

In Fig. 12, time traces of phase-averaged normalized surface pressure signals [see Eq. (2)] are presented. The data were acquired at three Reynolds numbers and at the two inlet freestream turbulence levels. The Reynolds number increases from the top to the bottom of the page with low turbulence intensity cases on the left. In each of the plots, the lowest trace is closest to the blade leading edge.

At the lowest Reynolds number and at the lower turbulence intensity, the surface pressure oscillations persist as far as the trailing edge. In the case of steady flow (see Fig. 2), reducing the Reynolds number results in a longer separation bubble, due to a delayed onset of transition in the separated shear layer. In the case of unsteady flow, the extended length of the separated laminar shear layer allows the vortices to penetrate farther downstream. In addition, more vortices form as the flow progresses. This is because the wake moves faster than the vortices and so can create additional perturbations downstream of the initial ones in the extended laminar shear layer. When increasing the Reynolds number the reverse is true, transition in the shear layer occurs earlier and the pressure fluctuations decay after a shorter surface distance.

The effect of Reynolds number is also presented for the higher freestream turbulence level. In steady flow, due to the higher freestream turbulence, the transition occurred farther upstream and separation was avoided. Here, in the unsteady flow, at the corresponding cases of Reynolds number in Fig. 12, the transition occurs farther upstream for the higher turbulence cases. Therefore, the vortices exist over a shorter surface distance. Furthermore, at the

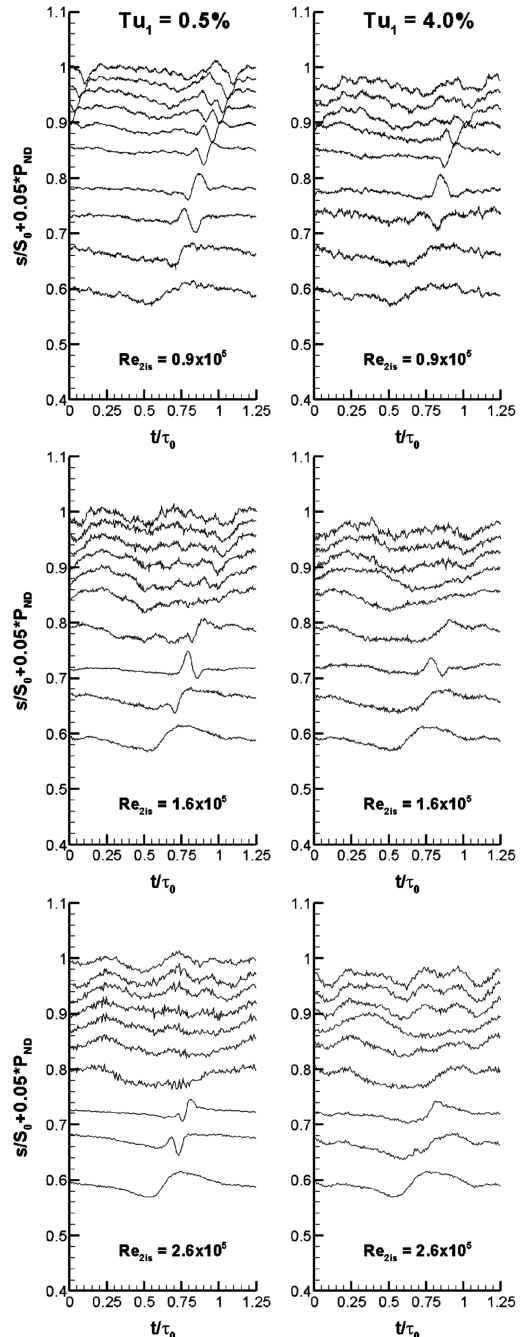


Fig. 12 Phase-averaged traces of unsteady surface pressure illustrating the effects of inlet freestream turbulence and Reynolds number at  $Re_{2is} = 0.9 \times 10^5$ ,  $1.6 \times 10^5$ , and  $2.6 \times 10^5$  for  $Tu_1 = 0.5\%$  (left) and  $Tu_1 = 4.0\%$  (right).

higher freestream turbulence, the appearance of the inflexional profiles occurs farther downstream, as indicated by the shape factor distribution in Fig. 7, and so there is less opportunity for the wake negative jet to interact with inflexional velocity profiles, and fewer vortices are formed. At the maximum Reynolds number case, with the higher freestream turbulence, roll-up vortices are not formed.

## V. Conclusions

The experimental results presented in this paper show that the inlet freestream turbulence and flow Reynolds number are both important and related factors in that they affect the unsteady suction-surface transition process on a T106A high-lift low-pressure turbine blade.

The LDA measurements in the blade passage at the higher level of freestream turbulence showed that the convection of the upstream wake is not significantly affected. A comparison of steady and

unsteady boundary layer LDA data acquired at the higher and lower levels of freestream turbulence showed that the higher freestream turbulence prevents the formation of the suction-surface separation bubble due to an earlier transition onset. Although in the case of the higher freestream turbulence, the wake contains higher turbulence levels, the turbulence in the wake induces bypass transition at a similar location to the case of the lower freestream turbulence level. This provides an important support for studies carried out at lower levels of freestream turbulence.

In the case of the lower freestream turbulence or low Reynolds number, the flow was observed to undergo laminar separation, which was periodically suppressed by the arrival of the wakes from upstream. The velocity perturbation associated with the negative jet behavior of the wake interacts with the separation bubble and forces the formation of coherent structures via a Kelvin–Helmholtz mechanism. The wake turbulence induces a bypass transition slightly later in time and space.

Increasing the level of inlet freestream turbulence delays in space the appearance of the inflexional profiles and moves the transition onset farther upstream. Therefore, there is less opportunity for the wake negative jet to interact with inflexional velocity profiles and fewer vortices are formed which subsequently decay faster. The surface pressure perturbations at the datum Reynolds number of  $1.6 \times 10^5$  induced by the vortices at the higher level of inlet turbulence are equal to 10% of exit dynamic pressure peak to peak, which is one-third of those observed in the lower turbulence case.

At the higher Reynolds number in both freestream turbulence cases, the transition in the shear layer occurs earlier. This shortens the length of the shear layer. Hence, fewer roll-up vortices formed, and the associated pressure fluctuations decay over a shorter surface distance. For the highest Reynolds number case, with the higher freestream turbulence intensity, roll-up vortices are not observed.

### Acknowledgments

The work reported in this paper was conducted as part of the project on “Unsteady Transitional Flows in Turbomachines” (UTAT), which was funded by the European Commission under contract number G4RD-CT-2001-00628. The authors want to thank Trevor Chandler, Alistair Ross, and David Grey who prepared the test facility.

### References

- [1] Curtis, E. M., Hodson, H. P., Banieghbal, M. R., Howell, R. J., and Harvey, N. W., “Development of Blade Profiles for Low Pressure Turbine Applications,” *Transactions of the ASME Journal of Turbomachinery*, Vol. 119, No. 3, July 1997, pp. 531–538.
- [2] Halstead, D. E., Wisler, D. C., Okiishi, T. H., Walker, G. J., Hodson, H. P., and Shin, H. W., “Boundary Layer Development in Axial Compressors and Turbines. Part 1 of 4: Composite Picture,” *Transactions of the ASME Journal of Turbomachinery*, Vol. 119, No. 1, 1997, pp. 114–127; also “Boundary Layer Development in Axial Compressors and Turbines. Part 3 of 4: Turbines,” *Transactions of the ASME Journal of Turbomachinery*, Vol. 119, No. 2, 1997, pp. 225–237.
- [3] Stieger, R., and Hodson, H., “The Transition Mechanism of Highly Loaded LP Turbine Blade,” *Journal of Turbomachinery*, Vol. 126, No. 4, Oct. 2004, pp. 536–543. doi:10.1115/1.1773850
- [4] Vera, M., Hodson, H. P., and Vasquez, R., “The Effects of a Trip Wire and Unsteadiness on a High-Speed Highly Loaded Low-Pressure Turbine Blade,” *Journal of Turbomachinery*, Vol. 127, No. 4, Oct. 2005, pp. 747–754. doi:10.1115/1.1934446
- [5] Hilgenfeld, L., and Pfitzner, M., “Unsteady Boundary Layer Development due to Wake Passing Effects on a Highly Loaded Linear Compressor Cascade,” ASME Paper GT2004-53186, 2004.
- [6] Schubauer, G. B., and Klebanoff, P. S., “Contribution of the Mechanics of Boundary-Layer Transition,” NACA TN 3489, 1955, pp. 1–31; also NACA Rept. 1289, 1955.
- [7] Schulte, V., and Hodson, H. P., “Unsteady Wake-Induced Boundary Layer Transition in High Lift LP Turbines,” *Journal of Turbomachinery* Vol. 120, Jan. 1998, pp 28–35.
- [8] Halstead, D. E., “Flowfield Unsteadiness and Turbulence in Multistage Low Pressure Turbines,” *Conference on Boundary Layer Transition in Turbomachines*, NASA CP 1998-206958, 7–10 Sept. 1997, pp. 237–250, <http://gltrs.grc.nasa.gov/reports/1998/CP-1998-206958.pdf>.
- [9] Binder, A., Schröder, T., and Hourmouziadis, J., “Turbulence Measurements in a Multistage Low-Pressure Turbine,” *Journal of Turbomachinery*, Vol. 111, 1989, pp 153–161.
- [10] Roach, P. E., “The Generation of Nearly Isotropic Turbulence by Means of Grids,” *International Journal of Heat and Fluid Flow*, Vol. 8 No. 2, June 1987, pp. 82–92. doi:10.1016/0142-727X(87)90001-4
- [11] Stieger, R., Hollis, D., and Hodson, H., “Unsteady Surface Pressures due to Wake-Induced Transition in a Laminar Separation Bubble on a Low-Pressure Cascade,” *Journal of Turbomachinery*, Vol. 126, No. 4, 2004, pp 544–550. doi:10.1115/1.1773851
- [12] Hodson, H. P., Huntsman, I., and Steele, A. B., “An Investigation of Boundary Layer Development in a Multistage LP Turbine,” *Transactions of ASME Journal of Turbomachinery*, Vol. 116, No. 3, July 1994, pp 375–382.
- [13] George, W. K., “Limitations to Measuring Accuracy Inherent in the Laser-Doppler Signal,” *Proceedings of the LDA Symposium Copenhagen*, 1976, pp. 20–63 (A76-45326 23-35).
- [14] Stieger, R. D., and Hodson, H. P., “The Unsteady Development of a Turbulent Wake Through a Downstream Low-Pressure Turbine Blade Passage,” *Journal of Turbomachinery*, Vol. 127, No. 2, April 2005, pp. 388–394. doi:10.1115/1.1811094
- [15] Walker, G. J., “Transitional Flow on an Axial Turbomachine Blading,” *Journal of Propulsion and Power*, Vol. 27, No. 5, May 1989, pp. 595–602.

A. Prasad  
Associate Editor